BJR

https://doi.org/10.1259/bjr.20180759

Received: 31 August 2018 | Revised: 02 January 2019 | Accepted: 16 January 2019

Cite this article as:
Cohen J, Anvari A, Samanta S, Poirier Y, Soman S, Alexander A, et al. Mild hyperthermia as a localized radiosensitizer for deep-seated tumors: investigation in an orthotopic prostate cancer model in mice. *Br J Radiol* 2019; **92**: 20180759.

SMALL ANIMAL IGRT SPECIAL FEATURE: FULL PAPER

Mild hyperthermia as a localized radiosensitizer for deep-seated tumors: investigation in an orthotopic prostate cancer model in mice

JUSTIN COHEN, AKBAR ANVARI, SANTANU SAMANTA, YANNICK POIRIER, SANDRINE SOMAN, ALLEN ALEXANDER, MAIDA RANJBAR, RAMILDA PAVLOVIC, ANDREW ZODDA, ISABEL L JACKSON, JAVED MAHMOOD, ZELJKO VUJASKOVIC and AMIT SAWANT

Department of Radiation Oncology, University of Maryland School of Medicine, Baltimore, MD, USA

Address correspondence to: Dr Amit Sawant
E-mail: *asawant@som.umaryland.edu*

Objective: Non-ablative or mild hyperthermia (HT) has been shown in preclinical (and clinical) studies as a localized radiosensitizer that enhances the tumoricidal effects of radiation. Most preclinical *in vivo* HT studies use subcutaneous tumor models which do not adequately represent clinical conditions (*e.g.* proximity of normal/critical organs) or replicate the tumor microenvironment—both of which are important factors for eventual clinical translation. The purpose of this work is to demonstrate proof-of-concept of locoregional radiosensitization with superficially applied, radiofrequency (RF)-induced HT in an orthotopic mouse model of prostate cancer.

Methods: In a 4-arm study, 40 athymic male nude mice were inoculated in the prostate with luciferase-transfected human prostate cancer cells (PC3). Tumor volumes were allowed to reach 150–250 mm^3 (as measured by ultrasound) following which, mice were randomized into (i) control (no intervention); (ii) HT alone; (iii) RT alone; and (iv) HT + RT. RF-induced HT was administered (Groups ii and iv) using the Oncotherm LAB EHY-100 device to achieve a target temperature of 41 °C in the prostate. RT was administered ~30 min following HT, using an image-guided small animal radiotherapy research platform. In each case, a dual arc plan was used to deliver 12 Gy to the target in a single fraction. One animal from each cohort was euthanized on Day 10 or 11 after treatment for caspase-9 and caspase-3 Western blot analysis.

Results: The inoculation success rate was 89%. Mean tumor size at randomization (~16 days post-inoculation) was ~189 mm^3 . Following the administration of RT and HT, mean tumor doubling times in days were: control = 4.2; HT = 4.5; RT = 30.4; and HT + RT = 33.4. A significant difference (p = 0.036) was noted between normalized nadir volumes for the RT alone (0.76) and the HT + RT (0.40) groups. Increased caspase-3 expression was seen in the combination treatment group compared to the other treatment groups.

Conclusion: These early results demonstrate the successful use of external mild HT as a localized radiosensitizer for deep-seated tumors.

Advances in knowledge: We successfully demonstrated the feasibility of administering external mild HT in an orthotopic tumor model and demonstrated preclinical proof-of-concept of HT-based localized radiosensitization in prostate cancer radiotherapy.

INTRODUCTION

Prostate cancer is the second most frequent cancer among males worldwide.[1,2] Most cases are locoregional disease, with excellent prognosis; 5-, 10-, and 15 year relative survival rates are 99%, 98%, and 96%, respectively. Among patients treated for locoregional disease, approximately one-third receive some form of radiation therapy (RT).[3] Given the high rates of long-term survival of these patients, increased interest has focused on long-term post-RT toxicities, which include radiation-induced erectile dysfunction (RiED), bowel dysfunction, and urinary dysfunction.[4] Mounting evidence from clinical studies, including the Prostate Cancer Outcomes Study[4] and the recently matured multi institutional Phase III randomized ProtecT trial,[5] indicates that patients with posttreatment side-effects consistently experience moderate-to-severe loss of quality of life (QoL).

Approaches to mitigate post-RT toxicity are based on: (a) dosimetric avoidance of critical structures through more frequent image guidance, RT plan optimization, and in-room real-time motion monitoring, as well as real-time adaptive dose delivery[6]; (b) phosphodiesterase Type

5 inhibitors to mitigate ED[7,8]; (c) radiation response modifiers for radiosensitization of the tumor[9–12] or radioprotection of normal tissues; these modifiers include amifostine (rectal toxicity),[13,14] famotidine (bowel toxicity),[15] and curcumin (urinary toxicity).[16,17]

Radiosensitizers are of particular interest because they aim to achieve local control comparable to that of standard of care at a significantly lower radiation dose to the tumor, thereby reducing the probability of RT-induced toxicity to surrounding critical structures. A number of radiosensitizers have been under investigation for localized prostate cancer, including heat shock protein 90 inhibitors (ganetespib, SNX-5422, HSP990), vascular endothelial growth factor receptor and platelet-derived growth factor receptor inhibitors (sunitinib, sorafenib), Src kinase inhibitors (dasatinib), and mammalian target of rapamycin pathway inhibitors (everolimus).[9–12] The main challenge with radiosensitizers is that most are systemically administered, and it is difficult to achieve high levels of specificity—the ability to distinguish between and selectively target tumor tissue rather than normal tissue.[18]

Androgen deprivation therapy (ADT), which is often administered in combination with RT for early-stage prostate cancer, has also been shown in *in vitro* studies to elicit a radiosensitization effect.[19] Radiation results in an increase in androgen receptor (AR) activity, which has been shown to cause biochemical relapse in human patients. *In vitro* and *in vivo* preclinical studies suggest that inhibiting AR activity through approaches such as ADT can reduce the probability of disease relapse. In the context of erectile function, a recent study from Washington University showed that ADT + RT results in poorer 2-year outcomes in terms of sexual function compared to RT alone.[20]

An attractive strategy to supplant or potentially complement systemic radiosensitizers is the use of non-ablative hyperthermia (HT), often termed as mild HT (40–45°C), as a localized radiosensitizer. HT-induced radiosensitization has been shown to occur via several mechanisms. Mechanisms such as vasodilation (resulting in increased oxygenation of the tumor), denaturing of DNA repair proteins that increase cell death following sublethal damage, and triggering of multiple local and systemic immune responses are observed at temperatures ≥ 39°C, and at slightly more elevated temperatures,≥42°C, radiosensitization is further enhanced due to HT-induced cytotoxicity.[21] The synergistic effect of hyperthermia and radiation occurs over a relatively wide window both before and after irradiation, approximately ±8 h in small animals, with the peak thermal enhancement ratio (TER = tumor control at elevated temperature *vs* tumor control at room temperature, for a given radiation dose) observed at ±30 min.[22]

Locoregional radiosensitization with superficially applied mild HT has been demonstrated preclinically as well as in a number of multicenter clinical trials, with promising results (better local control and/or reduced toxicity) reported in Phase III studies for cancers in the breast, cervix, bladder, and head/neck. A comprehensive review of HT + RT clinical trials has been published by Peeken et al.[23] Several Phase I and II studies of HT + RT for treatment of prostate cancer have been conducted, with some showing promising results in terms of overall survival,[24,25] whereas others reported no significant improvement in overall survival or quality of life measures.[26,27]

To better understand the biologic and technical aspects of HT + RT (as well as potential trimodality regimens involving HT + RT + ADT) in the treatment of prostate cancer, several preclinical investigations have been conducted in small animal models. A comprehensive literature review is outside the scope of this article, but the following are representative examples of these preclinical studies. Lein et al studied laser-induced HT to a temperature of 46.5°C in subcutaneous and orthotopic rat models and found that subcutaneous models systematically overestimated HT + RT–induced tumor growth inhibition compared to corresponding orthotopic models. In an investigation of magnetic fluid HT in an orthotopic Dunning rat model of prostate cancer, Johannsen et al reported that HT + RT was significantly more effective than RT alone in tumor growth reduction, and that an HT + 20 Gy radiation dose achieved comparable tumor growth inhibition to 60 Gy of RT alone.[28] The authors of this study were able to achieve an ablative dose, with a mean maximal intratumoral temperature of 58.7°C. Attaluri et al reported investigations of magnetic nanoparticle-induced HT to a temperature of 43.0°C combined with RT in a subcutaneous mouse model of prostate cancer.[29] More recently, Janati Esfahani et al reported significant radiosensitization with HT up to 43.0°C + RT compared to RT alone in a spheroid culture of DU145 prostate cancer cells.[30]

Compared to HT techniques such as transrectal HT or intratumoral injection of nanoparticles, radiofrequency (RF)-induced HT is much less invasive and potentially easier to translate into clinical practice. However, to our knowledge no investigations have evaluated RF-induced HT in deep-seated tumors. The objective of this study was to develop a preclinical orthotopic prostate cancer model in nude mice and present proof-of-concept results on radiosensitization resulting from external RF-induced HT.

METHODS AND MATERIALS

Study design

Following approval from our Institutional Animal Care and Use Committee, a 4-arm study was performed with forty 6–8 week-old male Foxn1^{nu} nude mice (The Jackson Laboratory; Bar Harbor, ME).

Cell culture

PC3-Luc prostate cancer cells were cultured in Minimum Essential Media (MEM) consisting of 10% (V/V) fetal bovine serum, 1% penicillin–streptomycin in an atmosphere of 95% air/5% CO_2 at 37°C, and seeded at 10^5 cells per well in six well plates, followed by the addition of 0.5 ml of hexadimethrine bromide to each of the growing cells. Thirty to hundred 30 μL of yellow fluorescent protein luciferase lentivirus were added to the wells in various titers. After 48 h of incubation, the cells were harvested for transduction using flow cytometry. Yellow fluorescent protein luciferase transduction in PC3 cells at the rate of >90% was selected and cultured for further use.

Figure 1. Surgical procedure for orthotopic tumor implantation in prostate. A nude mouse is shown. (A) Midline abdominal incision was followed by (b) identification of bladder and prostate. (C) Cell solution was injected into the ventral lobe of the prostate, followed by (D) closure of the abdominal musculature and closure of the skin. (E) Close-up view showing the relative locations of the mouse bladder and the prostate.

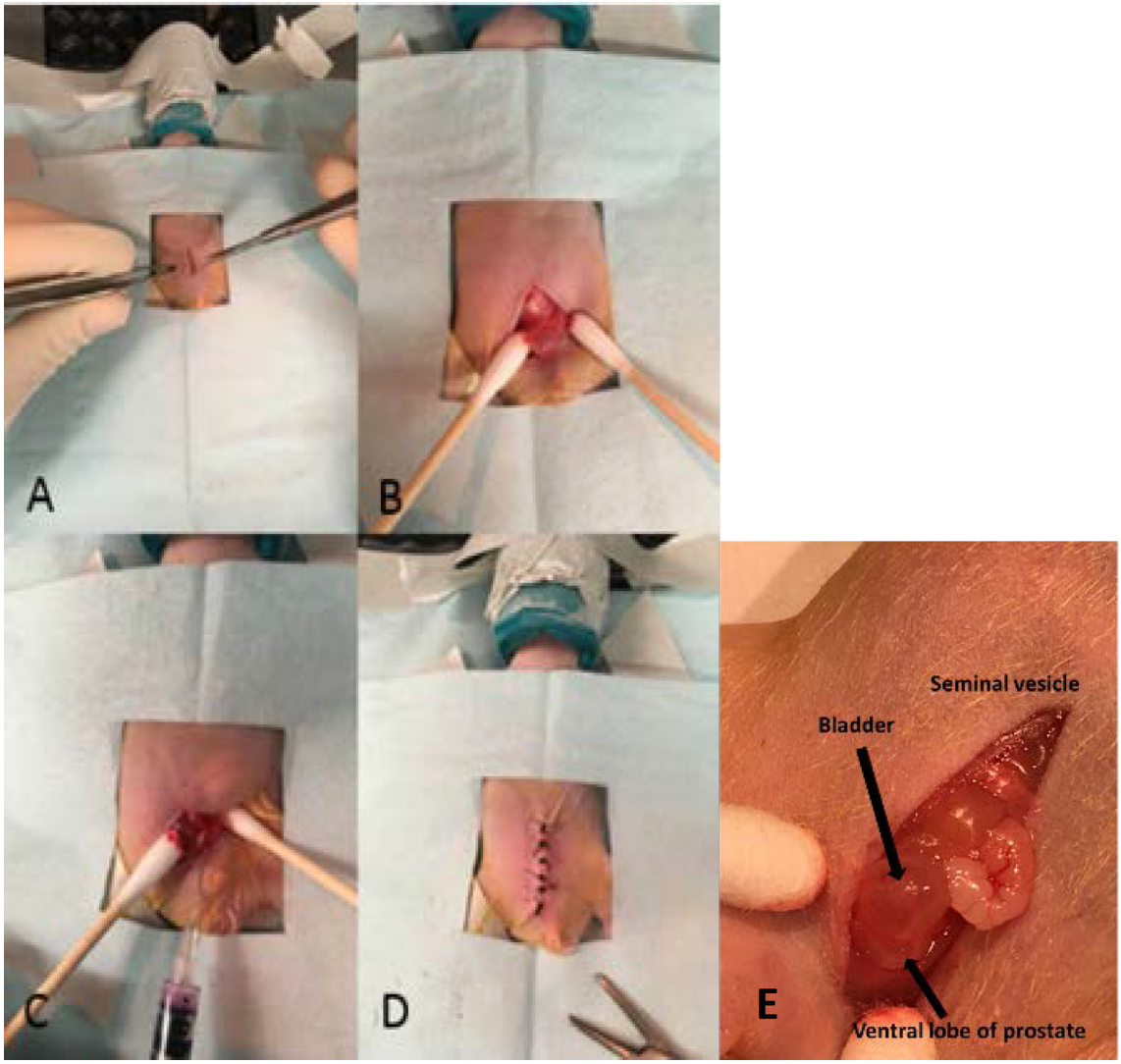

Tumor inoculation

Orthotopic implantation was performed under anesthesia with isoflurane on all 40 mice (isoflurane was the only anesthetic agent used in this study). All tumor inoculations were performed within 45 min of cell trypsinization. Figure 1 shows key steps in the procedure. A 5–10 mm low midline abdominal incision was made, followed by an incision through the abdominal musculature (Figure 1a). The bladder was then visualized to the depth of the incision. Light pressure was applied with cotton-tipped applicators on both sides of the bladder, pushing it up and out of the pelvis. The ventral lobe of the prostate was identified just inferior to the bladder (Figure 1b). A second individual then lightly grasped the bladder with two cotton-tipped applicators and applied gentle traction superiorly, providing countertraction during the injection, thus facilitating penetration of the needle into the prostate. Injection was performed using a 29-gauge needle (Figure 1c). A total volume of 20 μL were injected (1:1 Matrigel; Corning Incorporated, Corning, NY; and media) with 1 $\times 10^5$ cells. A cotton-tipped applicator was placed onto the injection site as the needle was removed from the prostate, ensuring minimal leakage of injected solution. The abdominal musculature was closed with 5–0 polyglycolic acid absorbable suture, and the skin was closed with 4–0 silk (Figure 1d). A close-up of the surgically exposed bladder and prostate is shown in Figure 1e. Carprofen was used for analgesia for 3 days post-operatively.

Tumor growth monitoring and randomization

Tumor inoculation and growth were monitored using two imaging modalities. Tumor inoculation was confirmed 7 days after surgery with bioluminescence imaging (BLI) using the IVIS Lumina system (Xenogen, Alameida, CA). Because BLI signals are sensitive to optical scatter, especially in orthotopic tumors, this modality was used primarily for its high sensitivity (*i.e.* identifying signal *vs* no signal). Quantitative characterization of

Figure 2. (a) Experimental setup showing an anesthetized mouse being administered hyperthermia using the Oncotherm EHY-100 RF-hyperthermia system. (b) Close-up view showing the positioning of the heating electrode on the ventral surface of the mouse and the rectally inserted temperature probe. (c) Change in rectal and skin temperature with hyperthermia administration. The right-hand side *y*-axis shows the power setting on the Oncotherm system.

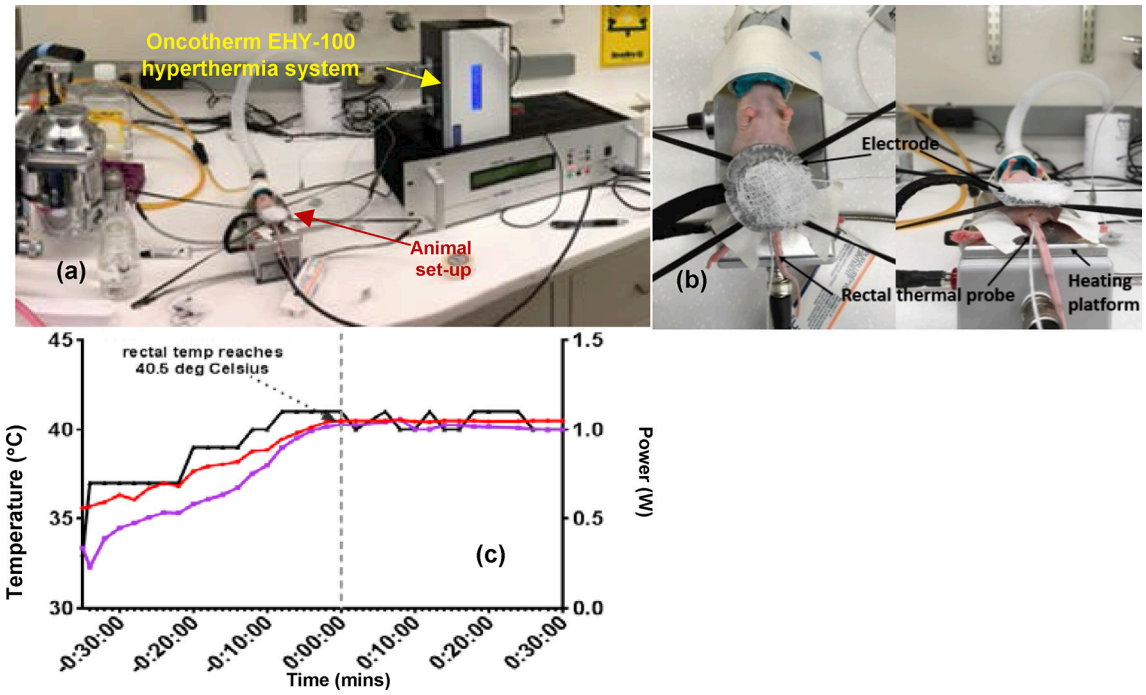

tumor growth was performed using ultrasound imaging (VisualSonics 2100, Toronto, Canada) with a linear-array transducer in B-mode with 30 MHz center frequency. Mice were anesthetized and placed in the supine position. Images of the tumor were obtained twice each week, with the transducer head in the axial and sagittal positions. Volumes were calculated assuming the tumors to be ellipsoid

$$\left(V = \frac{\pi}{6} \times L \times W \times H\right),$$

where V, L, W and H represent volume, length, width and height, respectively. Tumors were allowed to grow to a size of 150–250 mm^3, after which each animal was assigned to one of four groups: control (no treatment), HT alone, RT alone, or HT followed by radiation (HT +RT).

Hyperthermia

HT was delivered to each animal in the HT-only and HT + RT groups using the Oncotherm LAB EHY-100 (Oncotherm, Budaörs Hungary) device (Figure 2), which utilizes RF (13.56 MHz, 0–80 W). Following anesthesia, each animal was placed supine on a rectangular grounded electrode initialized to a temperature of ~38°C. A flexible circular electrode with a diameter of 2.5 cm was placed over the pelvis. A thermal probe was placed between the circular electrode and the skin to monitor the skin temperature during treatment. A thin layer of ultrasound gel was placed between the circular electrode and the pelvis to improve RF coupling, thereby lowering the risk of eddy currents and consequent skin burns. Rectal temperature, obtained via a second thermal probe, was used as a surrogate for prostate temperature because of the anatomic proximity of the two structures. As an additional measure to prevent skin burns, a piece of dampened gauze was placed over the circular electrode. HT treatment was initiated at 0.3 W. The power was slowly raised until the rectal temperature was ~40.5°C. The desired temperature was achieved at ~1 W (Figure 2b). For each animal, HT was administered for 30 min.

To validate the use of rectal temperature as a surrogate for prostate temperature, a non-survival surgery was performed on one animal, where a thermal probe was placed directly into the prostate tumor. It was observed that, during the warm-up phase, the rectal temperature was slightly higher than that of the prostate. After ~14 min, the temperatures equalized at 39.70°C. After ~18 min, when the rectal temperature of 40.50°C was reached, the prostate temperature was ~40.76°C.

Radiotherapy

All animal irradiations were performed on the small animal radiation research platform (SARRP; Xstrahl, Atlanta, GA). The system incorporates a cone beam CT (CBCT) image guidance system, a 3D planning system (Muriplan, Xstrahl, Atlanta, GA), and CBCT-guided three-dimensional localization prior to delivery of each treatment fraction. At our institution, this irradiator is calibrated monthly and annually by a clinical medical physicist according to the American Association of Physicists in Medicine Task Group 61 guidelines for kilovoltage X-ray dosimetry in RT.[31] The calibrations are performed using a PTW TN30013 Farmer-type ionization chamber (PTW; Freiburg, Germany) of 0.6 cm^3 volume with a calibration traceable to the

Figure 3. (A) Coronal and (B) axial CBCT slices showing the bladder filled with contrast. (C–F) Representative dual-arc RT plan delivering 12 Gy to the prostate using a 2 cm collimator. Portal images show (G) anteroposterior and (H) lateral beams for animal treatment position verification. RT, radiation therapy.

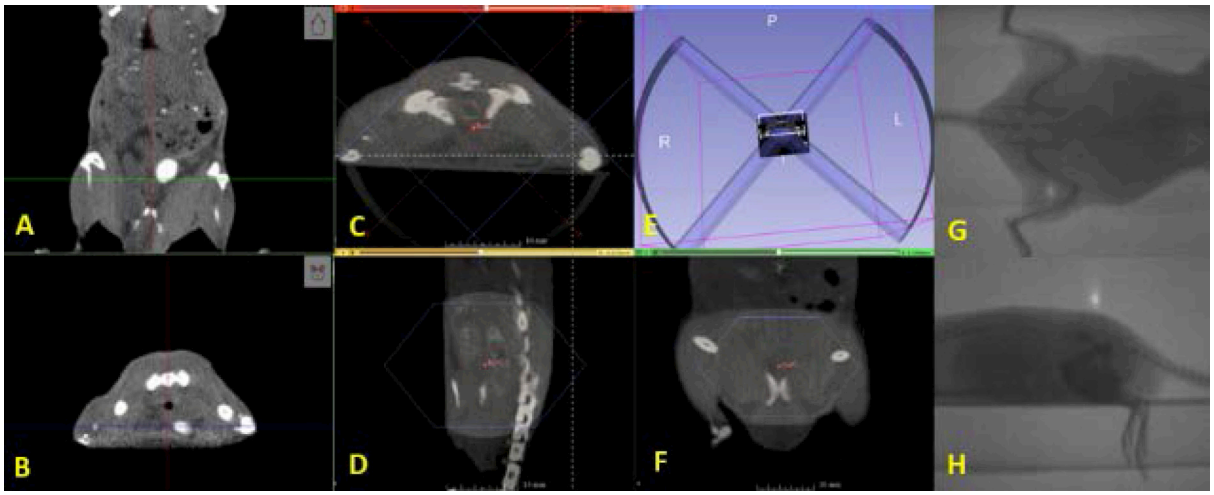

U.S. National Institute of Standards and Technology. The irradiator nominal open-field dose rate under calibration conditions (at a depth of 2 cm in solid water and source-to-surface distance of 33 cm) was 3.57 Gy/min.

For each animal receiving RT, volumetric images were acquired using the CBCT (60 kVp, 0.8 mA, 720 projections, 1 mm Al filter). Because the SARRP CBCT does not have adequate soft-tissue contrast resolution to directly visualize the mouse prostate, we performed an image-based validation in a test animal which was administered iohexol via the tail vein (Figure 3a,b). The contrast agent enabled us to visualize the bladder, which is adjacent to the prostate. The target was defined as the region posterior and inferior to the bladder, between the bladder and rectum, distal to the pelvic bones in the coronal CT image, and ventral to the pelvic bones in the axial CT image (Figure 4). For the remaining animals undergoing imaging and RT, the location of the prostate was estimated without contrast, using the relative positions of bony landmarks and soft tissue structures, as identified in the test animal (Figure 3a,b).

A target dose of 12 Gy to the prostate was planned and delivered in a single fraction with the following technique settings: 220 kVp, 13 mA, and a 0.15 mm Cu treatment filter. The RT plan included dual coplanar arcs (±45° to ±135°) using cones of 2 cm diameter and a source-to-axis distance of 35 cm. Irradiation times were optimized using Muriplan to account for animal-to-animal geometric variations but were in the 4.7–5.3 min range, for a dose rate ranging between 1.5 and 2.5 Gy/min. Animals were placed on the animal bed without additional immobilization.

Immediately prior to radiation delivery, treatment position was verified via anteroposterior (AP) and lateral portal images using the SARRP's electronic portal imaging device (Figure 5). On average, the complete procedure (*i.e.* imaging and RT delivery) was performed in less than 20 min per animal. For animals in the HT + RT treatment group, RT was delivered within 30 min following HT.

Electrophoresis and Western blot

Mice were euthanized at days 10 and 11 after treatment, and prostate tumors were immediately harvested. Samples representative of each group were frozen and stored at −20° for subsequent protein analysis and blotting. Samples from each treatment group were individually crushed and homogenized

Figure 4. (A) Ultrasound image reveals bladder implantation. (B) Example of multifocal disease: arrows pointing to two different tumor foci.

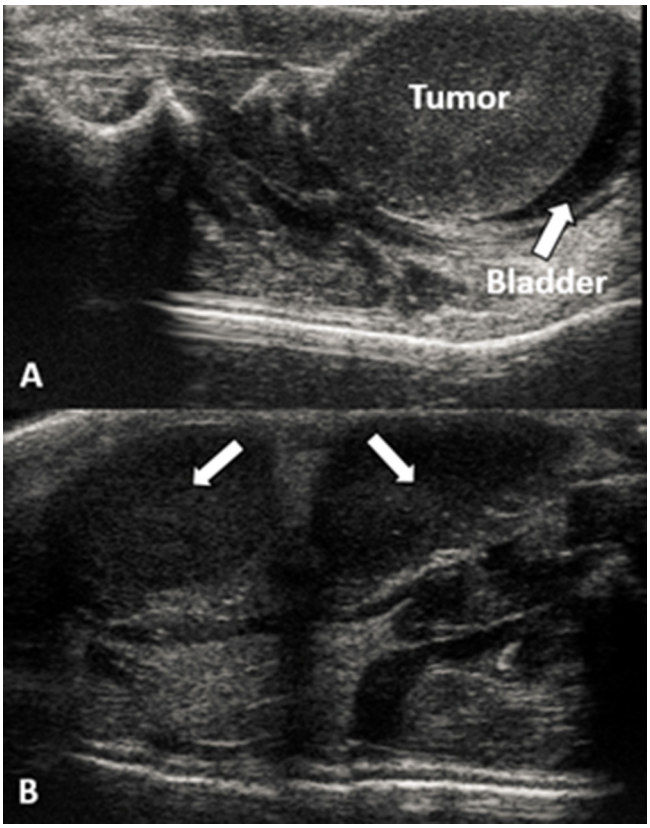

Figure 5. Tumor-growth curves for all four groups, volumes normalized at day 0 (RT delivery). RT, radiation therapy.

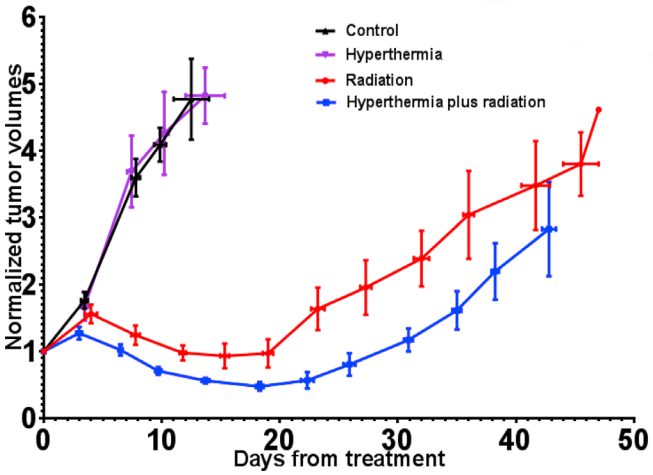

using radioimmunoprecipitation assay buffer. Extracted proteins were measured and loaded onto a tris/glycine (4–20%) gel at a 200 voltage for 25 min. Proteins were transferred onto a polyvinylidene difluoride membrane using the semi-dry Trans-Blot Turbo transfer system (Bio-Rad Laboratories), and blots were washed in phosphate-buffered saline–0.1% Tween 20 (PBST) three times, blocked in PBST–5% blotting-grade blocker for 30 min at room temperature. Primary antibodies were applied and incubated overnight at 4°C. Blots were washed three times in PBST, and the blot was rocked in secondary antibody for 1.5 h, followed by three washes and detection of horseradish peroxidase (HRP) using an enhanced chemiluminescence plus Western blotting kit (Amersham Biosciences; Piscataway, NJ). Antibodies used were caspase-3 rabbit monoclonal (1:1000; Cell Signaling), caspase-9 mouse monoclonal (1: 10,000; R &D Systems), anti-rabbit HRP-linked antibody (1:1000; Cell Signaling Technology), and stabilized goat antimouse HRP conjugated antibody (Pierce Biotechnology). Beta-actin, also known as a "housekeeping" protein, was used as a loading control to normalize the levels of protein detected by confirming that protein loading was the same across the gel. Bands were quantified using ImageJ Software (National Institutes of Health; Bethesda, MD).

H&E staining

Tumor samples harvested on days 10 and 11 were immediately stored in 10% formalin. Samples were incubated for 24 h and then embedded into paraffin. Paraffin blocks were then sliced and stained with hematoxylin and eosin to assess and evaluate tumor characteristics, including degrees of necrosis and fibrosis, and amounts of inflammatory infiltrates.

Data analysis

Data analyses were performed using GraphPad Prism program, v. 7 (San Diego, CA). Means of tumor nadir volumes were compared using a two-tailed T test.

RESULTS

Tumor uptake and growth were observed in all inoculated animals, as confirmed using BLI. However, ultrasound images indicated that three animals developed intrabladder foci (Figure 4a) and one developed multifocal disease (Figure 4b). These animals were excluded from the study, resulting in an overall inoculation success rate of ~89%. A total of 40 animals were chosen for randomization. Mean tumor size at earliest detection with ultrasound was 54.08 mm^3 (SEM = 5.99), mean maximum tumor diameter at earliest detection was 5.71 mm (SEM = 0.23), and mean tumor size at randomization was 189.06 mm^3 (SEM = 3.84). The mean time between inoculation and randomization/treatment: control = 16 days, HT alone = 16.7 days, RT alone = 15.8 days, and HT + RT=17 days. An analysis of variance revealed no significant difference between the groups ($p = 0.84$).

For the HT-related experiments, substantial effort was invested in optimizing the HT delivery technique in order to avoid toxicities. Toward this objective, an initial set of practice runs was performed. In these experiments, we observed skin burns in many animals after HT administration. These were almost completely mitigated by coupling the RF electrode to the skin via a thin layer of ultrasound gel. It is likely that without the gel non-uniform coupling between the electrode and skin occurred, leading to eddy currents and consequent severe heating at the electrode–skin interface. We also observed during these practice runs that some animals exhibited bladder injury. The cause was eventually traced to animal-to-animal variation in anatomy and therefore in thermal distribution along the rectal cavity. Thus, a probe inserted in the same position may be in the correct location in one animal while at a "cold spot" in another. In the latter case, the user would get an artificially low temperature reading and would continue ramping up the RF energy, thereby causing overheating of critical structures around the prostate. The thermal probe insertion technique was therefore modified, wherein the probe was moved from the proximal to the distal end in small increments to identify the location at which maximum temperature was registered. Placing the probe at this position (different for each animal) completely eliminated HT-related bladder toxicities.

Animals were euthanized either at the point when the tumor quadrupled in size following randomization/treatment, or when euthanasia criteria based on comorbidities were met. Table 1 shows the time to an increase in size to 1.5 times (×), and 2 × the tumor volume at time of treatment and Figure 5 shows the average normalized tumor volumes for each group as a function of time from treatment. After treatment, tumors in the RT

Table 1. Mean time in days for tumor growth for each group

Group	Days elapsed to relative tumor size (*n* animals)		
	1.00 ×	1.50 ×	2.00 ×
Control	0 ($n = 10$)	2.56 ± 0.45 ($n = 10$)	4.23 ± 0.56 ($n = 10$)
HT	0 ($n = 10$)	2.81 ± 0.46 ($n = 10$)	4.53 ± 0.90 ($n = 10$)
RT	0 ($n = 10$)	22.8 ± 2.84 ($n = 8$)	30.35 ± 4.05 ($n = 8$)
HT + RT	0 ($n = 10$)	31.91 ± 2.22 ($n = 7$)	33.43 ± 1.09 ($n = 4$)

HT, hyperthermia; RT, radiation therapy.
Numbers of animals at each time point are also given.

Figure 6. Western blot analysis of the effect of the control, HT (alone), RT (alone), and HT + RT on (A) caspase-9 and (B) caspase-3 expressions. Results are representative of three separate experiments. Band intensities were normalized and quantified using ImageJ analysis as shown in (C,D). HT, hyperthermia; RT, radiation therapy.

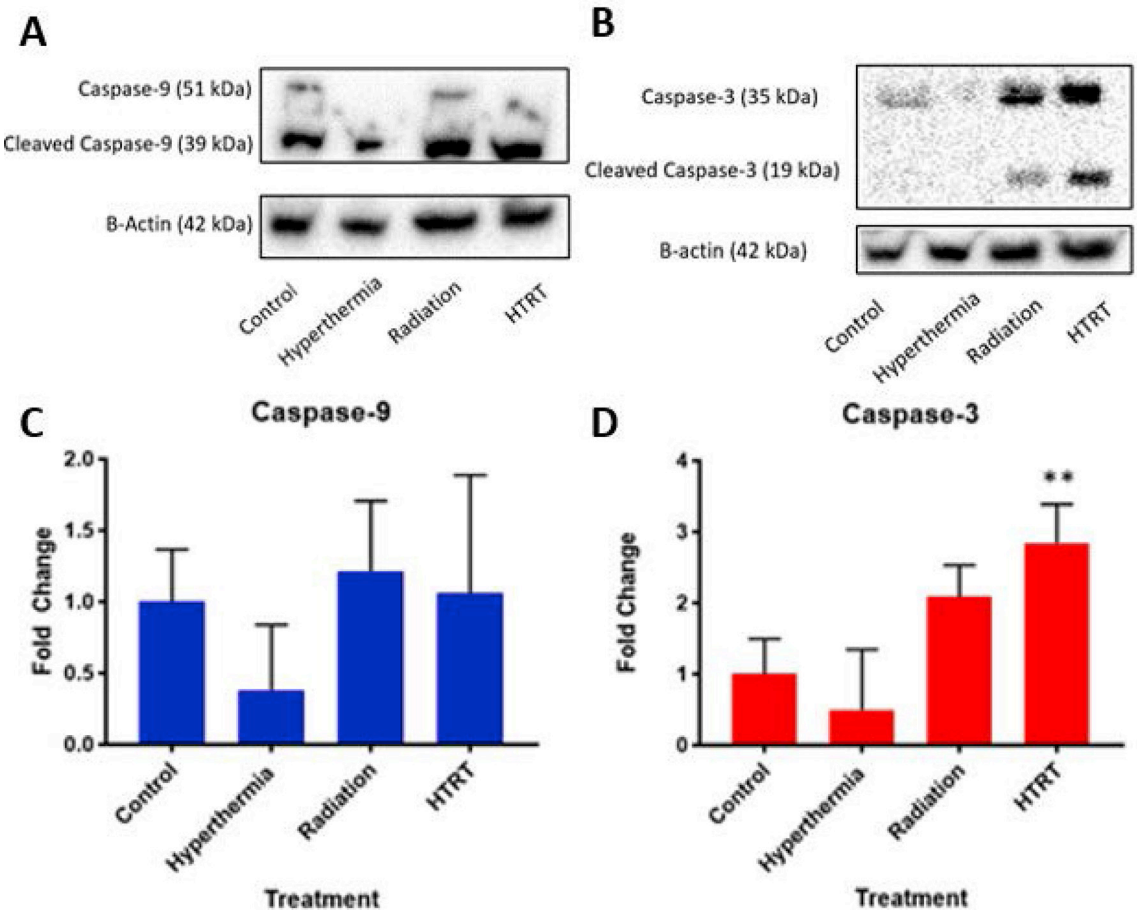

and HT + RT groups initially continued to grow but began to shrink after 3–7 days. The mean times to achieve 1.5 × tumor vol were 22.8 days for the RT group and 31.9 days for the HT + RT group ($p = 0.017$). Significant differences were also noted between the normalized nadir volumes for the RT (0.76 relative to day 0) and the HT + RT (0.40 relative to day 0) groups ($p = 0.036$). These early results suggest that external RF-induced mild HT can be administered to deep-seated tumors as a localized radiosensitizer.

To characterize apoptotic cell death in tumors after euthanasia, we measured caspase-9 and -3 using Western blot analysis. To confirm equal protein loading, each membrane was stripped and re-probed with antibeta-actin antibody. Figure 6 shows the results of expressions of whole or cleaved caspase-3 and –9 in controlled (no treatment), HT, or RT alone, and HT + RT. Compared to the control, RT, and HT + RT treated groups, the HT group tumors showed decreased caspase-9 expression (Figure 6a). However, no significant differences in expression of caspase-9 were observed between the control, RT, and HT + RT (Figure 6a,c) treated tumors. Consequently, little to no detectable caspase-3 expression was observed in the control group or HT-treated tumors. Increased expression of caspase-3 was seen in RT- and HT + RT–treated tumors, and HT + RT tumors showed significant ($p \leq 0.005$) increased expression compared to control tumors (Figure 6b,d). Because caspase-3 is an executioner caspase, an increase in expression represents a higher degree of apoptosis in the combination treatment arm.

We examined whether differences between our treatment groups could be appreciated on a microscopic level. One animal from each cohort was euthanized on day 10 or 11 after treatment. After H&E staining, tumor characteristics were evaluated by a pathologist blinded to the treatment groups of the given samples. All samples showed a high-grade pleomorphic malignancy. Focal mild fibrosis was seen in the sample treated with HT. Rare intratumoral lymphoid aggregates were seen in the sample treated with RT. Both focal mild fibrosis and lymphoid aggregates were seen in the HT + RT sample (Figure 7).

DISCUSSION

Mild HT represents an attractive localized radiosensitization technique that can help significantly improve the therapeutic ratio. An increase in the therapeutic ratio enables the achievement of local control comparable to current standard of care at a reduced radiation dose. Such dose reduction can significantly mitigate post-RT toxicity, thereby enhancing the post-treatment QoL for prostate cancer patients. In this work, we demonstrated

Figure 7. Histologic features of tumors. All images are H&E-stained slides at 200× magnification. (A) All specimens demonstrated a high-grade pleomorphic malignancy with ~0% necrosis. (B) Mild peritumoral lymphocytic response was present in all specimens. (C) A few scattered intratumoral lymphocytes were present in the RT specimen. Rare intratumoral lymphoid aggregates (D) and focal mild fibrosis (F) were seen in the HT+ RT specimen. (E) Focal mild fibrosis was present within the tumor for the HT specimen. HT,hyperthermia; RT, radiation therapy.

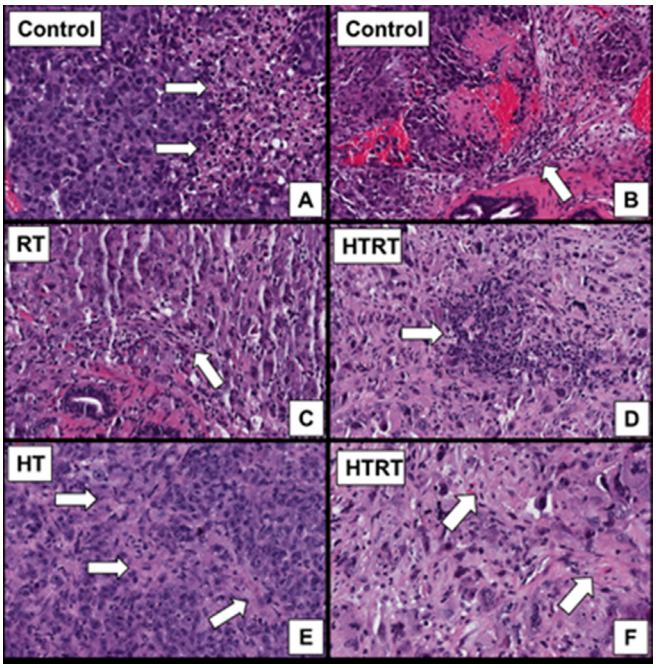

the feasibility of localized radiosensitization from external RF-induced mild HT in an orthotopic prostate cancer model in mice. Our early results suggest that it is possible to achieve significant radiosensitization in a deep-seated tumor using RF HT.

As stated in "Introduction", the various mechanisms of HT radiosensitization are temperature-dependent. Explicitly characterizing this relationship for each mechanism was beyond the scope of the present study. However, given the internal temperature achieved in these experiments (40–41°C), we can assume that mechanisms such as inhibition of DNA repair, vasodilation-induced oxygenation, and systemic immune responses were involved, while direct cell killing, which occurs at higher temperatures (>42°C), was unlikely to have occurred.

One of the predetermined endpoints of this study was quadrupling of tumor volume from that recorded at the time of treatment. However, in our RT and HT + RT groups, some animals met euthanasia criteria or were found deceased prior to this point. We determined, based on necropsy and/or ultrasound results, that all of these animals exhibited urinary outflow obstruction, secondary to compression from the tumor. This effect was observed even in animals in which tumors were still small. Notably, the obstruction was not observed in any of the animals in the control or HT groups, suggesting that it was not related to administration of HT alone. We speculate that the effect was observed in the RT and HT + RT groups because tumor growth was suppressed by therapeutic interventions. The pathophysiology leading to obstruction was similar to what is seen in benign prostatic hyperplasia (BPH). Bladder obstruction secondary to BPH is usually an insidious process. At the initial stages of BPH, the bladder is able to overcome the pressure within the compressed urethra. However, with continued and progressive obstruction, the bladder may eventually distend, leading to bladder damage. It is possible that a similar phenomenon occurred in the RT and HT + RT groups. To summarize, the control and the HT groups showed a rapid rate of tumor growth in which the tumors were capable of reaching the quadrupled tumor size euthanasia endpoint before bladder distension occurred. In contrast, the impaired tumor growth in the RT and HT + RT groups meant that the bladders had time to distend, triggering that euthanasia criteria before tumors could quadruple in size. It should be noted that this effect does not present a barrier to clinical translation, because it is unlikely to be observed in a clinical RT setting, with or without HT. In this study, the chosen RT dose was substantially lower than a clinically used tumoricidal dose, because we wanted to demonstrate relative growth delay in the HT + RT group.

An important lesson learned was to use an internal soft-tissue imaging modality (in our case, ultrasound) to monitor tumor growth in orthotopic models. Although BLI is sensitive in detecting signal, the modality is also quite sensitive to optical scatter, which can vary from measurement to measurement and animal to animal, making BLI unreliable in quantifying volume for deep-seated tumors. Furthermore, as seen in Figure 4, ultrasound imaging enabled us to visualize anomalous tumor inoculations, such as intrabladder implantation and multifocal disease. Neither could be reliably captured using BLI.

The impact of sequencing of HT and RT has been reported in the literature. The consensus, across a variety of tumor types, indicates that simultaneous use of HT and RT, *i.e.* hyperthermia during beam on, delivers the highest TER.[22,32,33] However, simultaneous HT + RT also sensitizes normal tissue and therefore does not result in overall therapeutic gain (TG = ratio of tumor control probability to normal tissue complication probability at a given radiation dose).[34] For this reason, sequential administration of HT and RT is recommended over simultaneous administration.

One possible limitation of this study is that while many preclinical studies (which use generally use subcutaneous tumor models) report on administering HT after RT,[32,34] in our experiments, which used an orthotopic prostate cancer model, HT was administered ~30 min before RT. The reason for this was mainly logistical, as it took ~30 min to reach the target temperature inside the prostate and another 30 min to maintain the temperature. However, given the time between HT and RT administration in our experiments (~30 min), data from other studies suggest that the difference in TG is unlikely to have been significant if the sequence were to be reversed. For example in a murine subcutaneous model of mammary carcinoma, Overgaard reported that for ~30 min between treatments, the TG values for HT→RT

(as was done in the present study) *vs* RT→HT were 1.12 *vs* 1.14, respectively.[34] Notably however, the same study also reported higher TG for RT→HT compared to HT→RT when the time between treatments modalities was longer (4–8 h).

Another possible limitation of this study was that we used an androgen-insensitive cell line, PC3. Although these cells are fast growing, they are not representative of the majority of clinically diagnosed prostate cancers, about 95% of which are androgen sensitive. Therefore, an androgen-sensitive cell line such as LNCaP may have been more suitable. However, these cells are extremely slow growing, and culturing them *in vitro* or *in vivo* is extremely challenging. Another limitation of our model was that we used nude mice. As stated in the Introduction, one of the mechanisms of HT-based radiosensitization is that HT elicits an immune response. Thus, our model could not capture this sensitization mechanism.

In conclusion, we were able to make iterative adjustments and optimize our HT treatment technique. As demonstrated, tumor growth and Western blot analysis of HT + RT demonstrated improved tumor control and increased apoptosis when compared to the control, HT, and RT groups. We expect that this model will open up promising opportunities for further testing and optimizing the use of HT in cancer treatment.

ACKNOWLEDGMENTS

We would like to thank Olivér Szász, PhD, András Szász, PhD, Gabor Andocs, DVM, PhD, at Oncothermia, who provided valuable guidance on the usage of the hyperthermia device. We would also like to thank Benjamin Deeley, MA, RDMS, at VisualSonics, who trained our research team in small animal ultrasound imaging. We are extremely grateful to Nancy Knight, PhD, who provided comments and edits that greatly improved the quality of this manuscript.

REFERENCES

1. Ferlay J, Soerjomataram I, Dikshit R, Eser S, Mathers C, Rebelo M, et al. Cancer incidence and mortality worldwide: sources, methods and major patterns in GLOBOCAN 2012. *Int J Cancer* 2015; **136**: E359–E386. doi: https://doi.org/10.1002/ijc.29210
2. Hassanipour-Azgomi S, Mohammadian-Hafshejani A, Ghoncheh M, Towhidi F, Jamehshorani S, Salehiniya H. Incidence and mortality of prostate cancer and their relationship with the human development index worldwide. *Prostate Int* 2016; **4**: 118–24. doi: https://doi.org/10.1016/j.prnil.2016.07.001
3. Löppenberg B, Sood A, Dalela D, Karabon P, Sammon JD, Vetterlein MW, et al. Variation in locoregional prostate cancer care and treatment trends at Commission on cancer designated facilities: a national Cancer data base analysis 2004 to 2013. *Clin Genitourin Cancer* 2017; **15**: e955–68. doi: https://doi.org/10.1016/j.clgc.2017.04.014
4. Resnick MJ, Koyama T, Fan KH, Albertsen PC, Goodman M, Hamilton AS, et al. Long-term functional outcomes after treatment for localized prostate cancer. *N Engl J Med* 2013; **368**: 436–45. doi: https://doi.org/10.1056/NEJMoa1209978
5. Donovan JL, Hamdy FC, Lane JA, Mason M, Metcalfe C, Walsh E, et al. Patient-reported outcomes after monitoring, surgery, or radiotherapy for prostate cancer. *N Engl J Med* 2016; **375**: 1425–37. doi: https://doi.org/10.1056/NEJMoa1606221
6. Choe KS, Liauw SL. Radiotherapeutic strategies in the management of low-risk prostate cancer. *Scientific World Journal* 2010; **10**: 1854–69. doi: https://doi.org/10.1100/tsw.2010.179
7. Zelefsky MJ, Shasha D, Branco RD, Kollmeier M, Baser RE, Pei X, et al. Prophylactic sildenafil citrate improves select aspects of sexual function in men treated with radiotherapy for prostate cancer. *J Urol* 2014; **192**: 868–74. doi: https://doi.org/10.1016/j.juro.2014.02.097
8. Pisansky TM, Pugh SL, Greenberg RE, Pervez N, Reed DR, Rosenthal SA, et al. Tadalafil for prevention of erectile dysfunction after radiotherapy for prostate cancer: the Radiation Therapy Oncology Group [0831] randomized clinical trial. *JAMA* 2014; **311**: 1300–7. doi: https://doi.org/10.1001/jama.2014.2626
9. Alcorn S, Walker AJ, Gandhi N, Narang A, Wild AT, Hales RK, et al. Molecularly targeted agents as radiosensitizers in cancer therapy--focus on prostate cancer. *Int J Mol Sci* 2013; **14**: 14800–32. doi: https://doi.org/10.3390/ijms140714800
10. Thakur MK, Heilbrun LK, Sheng S, Stein M, Liu G, Antonarakis ES, et al. A phase II trial of ganetespib, a heat shock protein 90 Hsp90) inhibitor, in patients with docetaxel-pretreated metastatic castrate-resistant prostate cancer (CRPC)-a prostate cancer clinical trials consortium (PCCTC) study. *Invest New Drugs* 2016; **34**: 112–8. doi: https://doi.org/10.1007/s10637-015-0307-6
11. Infante JR, Weiss GJ, Jones S, Tibes R, Bauer TM, Bendell JC, et al. Phase I dose-escalation studies of SNX-5422, an orally bioavailable heat shock protein 90 inhibitor, in patients with refractory solid tumours. *Eur J Cancer* 2014; **50**: 2897–904. doi: https://doi.org/10.1016/j.ejca.2014.07.017
12. Spreafico A, Delord JP, De Mattos-Arruda L, Berge Y, Rodon J, Cottura E, et al. A first-in-human phase I, dose-escalation, multicentre study of HSP990 administered orally in adult patients with advanced solid malignancies. *Br J Cancer* 2015; **112**: 650–9. doi: https://doi.org/10.1038/bjc.2014.653
13. Ménard C, Camphausen K, Muanza T, Sears-Crouse N, Smith S, Ben-Josef E, et al. Clinical trial of endorectal amifostine for radioprotection in patients with prostate cancer: rationale and early results. *Semin Oncol* 2003; **30**(Supplement 18): 63–7. doi: https://doi.org/10.1053/j.seminoncol.2003.11.016
14. Kouloulias VE, Kouvaris JR, Pissakas G, Mallas E, Antypas C, Kokakis JD, et al. Phase II multicenter randomized study of amifostine for prevention of acute radiation rectal toxicity: topical intrarectal versus subcutaneous application. *Int J Radiat Oncol Biol Phys* 2005; **62**: 486–93. doi: https://doi.org/10.1016/j.ijrobp.2004.10.043
15. Razzaghdoust A, Mozdarani H, Mofid B. Famotidine as a radioprotector for rectal mucosa in prostate cancer patients treated with radiotherapy: phase I/II randomized placebo-controlled trial. *Strahlenther Onkol* 2014; **190**: 739–44. doi: https://doi.org/10.1007/s00066-014-0602-8
16. Hejazi J, Rastmanesh R, Taleban F, Molana S. Ehtejab G. A pilot clinical trial of radioprotective effects of curcumin supplementation in patients with prostate cancer. *J Cancer Sci Ther* 2013; **5**: 320–4.

17. Schmidt KT, Figg WD. The potential role of curcumin in prostate cancer: the importance of optimizing pharmacokinetics in clinical studies. *Transl Cancer Res* 2016; **5**(S6): S1107–S1110. doi: https://doi.org/10.21037/tcr.2016.11.04
18. Citrin DE, Mitchell JB. Altering the response to radiation: sensitizers and protectors. *Semin Oncol* 2014; **41**: 848–59. doi: https://doi.org/10.1053/j.seminoncol.2014.09.013
19. Yao M, Rogers L, Suchowerska N, Choe D, Al-Dabbas MA, Narula RS, et al. Sensitization of prostate cancer to radiation therapy: Molecules and pathways to target. *Radiother Oncol* 2018; **128**: 283–300. doi: https://doi.org/10.1016/j.radonc.2018.05.021
20. Gay HA, Sanda MG, Liu J, Wu N, Hamstra DA, Wei JT, et al. External beam radiation therapy or brachytherapy with or without short-course neoadjuvant androgen deprivation therapy: results of a multicenter, prospective study of quality of life. *Int J Radiat Oncol Biol Phys* 2017; **98**: 304–17. doi: https://doi.org/10.1016/j.ijrobp.2017.02.019
21. Dewhirst MW, Vujaskovic Z, Jones E, Thrall D. Re-setting the biologic rationale for thermal therapy. *Int J Hyperthermia* 2005; **21**: 779–90. doi: https://doi.org/10.1080/02656730500271668
22. Crezee H, van Leeuwen CM, Oei AL, Stalpers LJ, Bel A, Franken NA, et al. Thermoradiotherapy planning: integration in routine clinical practice. *Int J Hyperthermia* 2016; **32**: 41–9. doi: https://doi.org/10.3109/02656736.2015.1110757
23. Peeken JC, Vaupel P, Combs SE. Integrating hyperthermia into modern radiation oncology: what evidence is necessary? *Front Oncol* 2017; **7**: 132. doi: https://doi.org/10.3389/fonc.2017.00132
24. Hurwitz MD, Hansen JL, Prokopios-Davos S, Manola J, Wang Q, Bornstein BA, et al. Hyperthermia combined with radiation for the treatment of locally advanced prostate cancer: long-term results from Dana-Farber Cancer Institute Study 94-153. *Cancer* 2011; **117**: 510–6. doi: https://doi.org/10.1002/cncr.25619
25. Maluta S, Dall'Oglio S, Romano M, Marciai N, Pioli F, Giri MG, et al. Conformal radiotherapy plus local hyperthermia in patients affected by locally advanced high risk prostate cancer: preliminary results of a prospective phase II study. *Int J Hyperthermia* 2007; **23**: 451–6. doi: https://doi.org/10.1080/02656730701553260
26. Yahara K, Ohguri T, Yamaguchi S, Imada H, Narisada H, Ota S, et al. Definitive radiotherapy plus regional hyperthermia for high-risk and very high-risk prostate carcinoma: thermal parameters correlated with biochemical relapse-free survival. *Int J Hyperthermia* 2015; **31**: 600–8. doi: https://doi.org/10.3109/02656736.2015.1062214
27. Van Vulpen M, De Leeuw JR, Van Gellekom MP, Van Der Hoeven J, De Graeff A, Van Moorselaar RJ, et al. A prospective quality of life study in patients with locally advanced prostate cancer, treated with radiotherapy with or without regional or interstitial hyperthermia. *Int J Hyperthermia* 2003; **19**: 402–13. doi: https://doi.org/10.1080/0265673031000063855
28. Johannsen M, Thiesen B, Gneveckow U, Taymoorian K, Waldöfner N, Scholz R, et al. Thermotherapy using magnetic nanoparticles combined with external radiation in an orthotopic rat model of prostate cancer. *Prostate* 2006; **66**: 97–104. doi: https://doi.org/10.1002/pros.20324
29. Attaluri A, Kandala SK, Wabler M, Zhou H, Cornejo C, Armour M, et al. Magnetic nanoparticle hyperthermia enhances radiation therapy: a study in mouse models of human prostate cancer. *Int J Hyperthermia* 2015; **31**: 359–74. doi: https://doi.org/10.3109/02656736.2015.1005178
30. Janati Esfahani A, Mahdavi SR, Shiran MB, Khoei S. The role of radiofrequency hyperthermia in the radiosensitization of a human prostate cancer cell line. *Cell J* 2017; **19**(Suppl 1): 86–95. doi: https://doi.org/10.22074/cellj.2017.4460
31. Ma CM, Coffey CW, DeWerd LA, Liu C, Nath R, Seltzer SM, et al. AAPM protocol for 40-300 kV X-ray beam dosimetry in radiotherapy and radiobiology. *Med Phys* 2001; **28**: 868–93. doi: https://doi.org/10.1118/1.1374247
32. Mittal B, Emami B, Sapareto SA, Taylor FH, Abrath FG. Effects of sequencing of the total course of combined hyperthermia and radiation on the RIF-1 murine tumor. *Cancer* 1984; **54**: 2889–97. doi: https://doi.org/10.1002/1097-0142(19841215)54:12<2889::AID-CNCR2820541213>3.0.CO;2-C
33. Horsman MR, Overgaard J. Hyperthermia: a potent enhancer of radiotherapy. *Clin Oncol* 2007; **19**: 418–26. doi: https://doi.org/10.1016/j.clon.2007.03.015
34. Overgaard J. Simultaneous and sequential hyperthermia and radiation treatment of an experimental tumor and its surrounding normal tissue in vivo. *Int J Rad Onc Biol Phys* 1980; **6**: 1507–17. doi: https://doi.org/10.1016/0360-3016(80)90008-5